# An overview on the airborne measurement in Nepal,-part 1: vertical profile of aerosol size-number, spectral absorption, and meteorology

Ashish Singh[1]*, Khadak S. Mahata[1], Maheswar Ruphaketi[1]*, Wolfgang Junkermann[2], Arnico K. Panday[3], Mark G. Lawrence[1]

[1]Institute for Advanced Sustainability Studies, Potsdam, Germany

[2]Institute of Meteorology and Climate Research, IMK-IFU, Garmisch-Partenkirchen, Germany

[3]International Centre for Integrated Mountain Development (ICIMOD), Lalitpur, Nepal

*Corresponding author: Ashish Singh (ashish.singh@iass-potsdam.de) and Maheswar Rupakheti (maheswar.rupakheti@iass-potsdam.de)

**Abstract**

The paper provides an overview of an airborne measurement campaign with a microlight aircraft, over the Pokhara Valley region, Nepal, a metropolitan region in the central Himalayan foothills. This is the first aerial measurements in the central Himalayan foothill region, one of the polluted but relatively poorly sampled regions of the world. Conducted in two phases (in May 2016 and December 2016-January 2017), the goal of the overall campaign was to quantify the vertical distribution of aerosols over a polluted mountain valley in the Himalayan foothills, as well as to investigate the extent of regional transport of emissions into the Himalayas. This paper summarizes results from first phase where test flights were conducted in May 2016 (pre-monsoon), with the objective of demonstrating the potential of airborne measurements in the region using a portable instrument package (size with housing case: 0.45 m x 0.25 m x 0.25 m, 15 kgs) onboard an ultralight aircraft (IKARUS-C42). A total of five sampling test flights were conducted (each lasting for 1-1.5 h) in the Pokhara Valley to characterize vertical profiles of aerosol properties such as aerosol number and size distribution (0.3-2 μm), total particle concentration (>14 nm), aerosol absorption (370-950 nm), black carbon (BC), and meteorological variables. Although some interesting observations were made during the test flight, the study is limited to a few days (and only a few hours of flight in total) and thus, the analysis presented may not represent the entire pollution-meteorology interaction found in the Pokhara Valley

The vertical profiles of aerosol species showed decreasing concentrations with altitude (815 to 4500 m a.s.l.); steep concentration gradient below 2000 m (a.s.l.) in the morning and mixed profiles (up to ca. 4000 m a.s.l.) in the afternoon. The near-surface (<1000 m a.s.l.) BC concentrations observed in the Pokhara Valley were much lower than pre-monsoon BC concentrations in the Kathmandu Valley, and similar in range to Indo-Gangetic Plain (IGP) sites such as Kanpur in India. The sampling test flight also detected an elevated polluted aerosol layer (around 3000 m a.s.l.) over the Pokhara Valley, which could be associated with the regional transport. The total aerosol and black carbon concentration in the polluted layer was comparable with the near-surface values (<1000 m a.s.l.). The elevated polluted layer was also characterized by high aerosol extinction coefficient (at 550 nm) and was identified as smoke and a polluted dust layer. The observed shift in the westerlies (at 20-30° N) entering Nepal during the test flight period could be an important factor for the presence of elevated polluted layers in the Pokhara Valley.

## 1. Introduction

The Himalayas and surrounding regions are one of the unique ecosystems in the world, with a great variety in the geography and socio-economics, and a notable significance in the context of regional and global environmental change. Areas in the foothills of the Himalayas still constitute large regions of rural populations along with pockets of rapidly growing cities. Consequently, there is a complex interaction among changing emission sources and their interaction with regional and global climate change. Among emitted air pollutants, the chemical and physical properties of aerosols have been linked to significant burdens of disease, to melting of glaciers, to crop loses, to hydrological changes and to cloud properties (Bollasina et al., 2011;Vinoj et al., 2014;Lau, 2014;Burney and Ramanathan, 2014;Brauer et al., 2012;Cong et al., 2015;Li et al., 2016).

Sources of aerosols in the Himalayas and the nearby Indo-Gangetic Plain (IGP) typically vary between urban, peri-urban and rural locations; fossil fuel and industrial emissions such as vehicles, brick kilns, waste burning, cement factories etc., are typically urban and peri-urban; biomass cookstove, agriculture and waste burning and forest fires are often linked to emissions from rural areas (Guttikunda et al., 2014;Venkataraman et al., 2006;Stone et al., 2010). Secondary chemical pathways also contribute to the aerosols in the ultrafine and accumulation-mode range via particle formation events (Venzac et al., 2008;Neitola et al., 2011).

Aerosol properties in the Himalayas have large spatial and temporal variations, especially in the pre-monsoon and monsoon season. These observed variations are influenced by emission sources, regional meteorology, and geography (Dey and Di Girolamo, 2010). The influence of aerosol particles on local and regional weather during these adjacent seasons has significant implications for timing, intensity and spatial distribution of the summer monsoon in the region (Bollasina et al., 2011;Ramanathan et al., 2001). Studies describing the aerosol-meteorology interaction are often missing in the Himalayan region partly due to lack of surface and airborne measurements of aerosol properties along with meteorology. Most past campaign-mode measurements in the Himalayan regions, to our knowledge, have been ground measurements, which have aided in evaluating aerosol properties, and their transformation and transport mechanisms (Shrestha et al., 2013;Shrestha et al., 2010;Ramana et al., 2004;Marcq et al., 2010;Panday and Prinn, 2009;Cho et al., 2017). Long-term continuous measurements of aerosols and meteorology are limited to a few stations in the High Himalayas, such as the recently discontinued Nepal Climate Observatory at Pyramid (NCO-P, 27.95° N, 86.81° E, 5050 m a.s.l.), a high altitude observatory located near basecamp of Mt. Everest. Columnar and satellite measurements such as AERONET and CALIPSO have provided a regional overview of aerosol type and vertical distribution, as well as

estimation of the aerosol heating rate in the atmospheric column (Kuhlmann and Quaas, 2010;Gautam et al., 2011;Pandey et al., 2017). However, these measurement techniques often suffer from large uncertainty and biases while retrieving the complex nature of the aerosols observed in the region (Jai Devi et al., 2011).

Regional meteorology in the 850-500 mb range plays an important role in the transformation and transport of aerosols from Western Asia to the IGP, the Himalayan foothills, the Himalayan and Tibetan Plateau region (Decesari et al., 2010;Marinoni et al., 2013;Lüthi et al., 2015). At these altitudes, synoptic- scale air masses are mostly westerly/northwesterly during the pre-monsoon and southwesterly/easterly during the monsoon. These air masses are often linked to dust aerosol transport during the pre-monsoon season from Western Asia into the Himalayas, including populated mountain valley such as Kathmandu and Pokhara Valley in Nepal. The transported dust aerosol also mixes with the primary emission (or anthropogenic aerosols) in the IGP and accumulates from northern to eastern IGP along the Himalayan foothills (Gautam et al., 2009b;Gautam et al., 2011). The total aerosol loading is often the highest during the pre-monsoon season in the IGP (Gautam et al., 2009a;Raatikainen et al., 2014), intensified further by weak surface/zonal winds and numerous open biomass burning and forest fires events (Kaskaoutis et al., 2012). The polluted aerosol layer in the IGP is advected into the Himalayas by synoptic-scale westerlies (~500 mb) and also by the valley wind circulation within or along the planetary boundary layer (PBL) (Lüthi et al., 2015). The advection is also facilitated by the strong updraft and PBL expansion (the highest in the pre-monsoon in the IGP) often mixing with the synoptic-scale westerlies (Raatikainen et al., 2014). Because of strong convective activity in the IGP, the polluted air masses near the surface are often lifted up to 5-7 km or higher (Kuhlmann and Quaas, 2010). In addition to the synoptic-scale transport, thermally-driven valley winds also enable the transport of humid and polluted air mass (with enhanced absorbing fraction) from IGP into the Himalayan foothills, and further up into the mountain valleys and elevated locations (Raatikainen et al., 2014;Lüthi et al., 2015;Gogoi et al., 2014;Putero et al., 2014;Decesari et al., 2010;Marcq et al., 2010). Strongly coupled with the expansion of the PBL in the IGP, the upslope movement of polluted air masses into the foothills and further east is characterized by late afternoon peaks in aerosol optical depth (AOD) in many measurement sites along the Himalayan range such as Hanle Valley (Ladakh, India), Mukteswar and Manora site (Nainital, India), Hetauda (Nepal), Langtang Valley (Nepal), Dhulikhel (Nepal), Kathmandu Valley (Nepal) and NCO-P (Nepal). The temporal and spatial extent of this observed “ventilation” at multiple locations could be indicative of a regional-scale transport than mesoscale (Gogoi et al., 2014;Raatikainen et al., 2014;Gautam et al., 2011;Putero et al., 2015;Marcq et al., 2010).

To date, there have been no observations of vertical distributions of aerosol and gaseous species carried out in the Himalayan region. Therefore, the airborne measurement campaign was designed to address two major questions: (i) what is the variation in the aerosol properties, notably the vertical distributions, over a polluted mountain valley, and (ii) what is the quantitative extent of regional transport of aerosols in the higher Himalayas? The campaign was carried out in two phases in the Pokhara Valley and surrounding areas in Nepal. In the first phase, test flights were conducted in May 2016 and in the second phase, intensive sampling flights were carried out in December 2016-January 2017. This paper provides an overview of the measurement campaign and results from the test flights in May 2016 which include snapshots of vertical profiles of aerosol size, number, and composition, along with meteorological parameters. The airborne measurements presented in this paper are supplemented with observations of local and regional meteorology, as well as satellite and ground-based column-integrated aerosol microphysics and radiative properties (see section 3.1.1 and 3.1.2, also Supplementary S7). A companion paper will follow with more detailed observations and results based on the intensive measurements carried out during December 2016-January 2017.

## 2. Ultralight measurements in Nepal

### *2.1. Details of the airborne measurement unit*

A single-engine two-seater microlight aircraft (IKARUS C-42, COMCO IKARUS, Germany) was used as the aerial platform. The technical specification of the aircraft includes approximately 4 h of flying time, a short take-off run, an additional payload of up to 50 kg, and it is suitable for small spiral movement in the air. The aircraft has a cruising speed of 165 $kmh^{-1}$, and a 5-6 $ms^{-1}$ rate of climb which makes it an appropriate aerial vehicle to perform measurements at altitudes within the PBL and as close as 50 m above ground level. More detail about the aircraft is available here (http://www.comco-ikarus.de/Pages/c42a-technik.php?lang=en). Its size, speed, and maneuverability offered a decent climb to the free troposphere to capture vertical profiles in the rough terrains of Nepal. The aircraft used for the study is operated by the Pokhara Ultralight Company for recreational flights around the Pokhara Valley.

The instrument package was specifically designed and tested for aerial measurements (Junkermann, 2001). Table 1 describes each instrument and the integration performed to prepare the package for the aerial deployment. The instrument package consists of a GRIMM OPS (optical particle spectrometer) model 1.108 for particle size distributions (0.3 to 20 µm, 16 size bins) with sampling frequency of 6 s,

and a TSI condensation particle counter (CPC) 3760 for total particle concentration (>14 nm) at 1 s resolution (See Figure S1 in the supplement). The package also included a Magee Scientific aethalometer (AE42) for aerosol absorption at seven different wavelengths (370 -950 nm). The instruments were reduced in weight for use on the aircraft. The CPC was operated with a constant mass flow and an internal direct current (DC) pump instead of the original flow regulation by a critical orifice. Meteorological parameters including temperature and dew point were sampled at a rate of 1 s using METEOLABOR (TPS3). All the sensors were connected to a modular computer (PC104) for data acquisition. The PC104 is also equipped with a Global Positioning System (GPS), and multiple serial and analog connectors. For inflight instrument checks and quick online overview of the atmospheric conditions, a small liquid crystal display (LCD) was also connected to the PC104 and placed in the cockpit areas for the flight crew. This display showed real-time aerosol number concentrations and meteorological parameters.

**Table 1. Instrument package deployed in the microlight aircraft**

The instrument package weighs approximately 15 kg and consumes <60 W, well within the power supply range of the aircraft battery. It is housed in an aluminum box (0.45 m x0.25 mx0.25 m) and can be easily integrated with a mobile platform such as the IKARUS (See Figure S1). In IKARUS, the instrument was placed in the rear section behind the seats which is otherwise almost empty or used for cargo, and only contains the fuel tank and supporting aluminum bars. The sample inlet line (internal diameter of 0.004 m or ~4.0 mm ID brass tubing) ran along the wingspan and was approximately 1.8 m (in length, sampling tube) from the cockpit. Once the sample line is inside the aircraft, it is distributed to all the aerosol instruments using a simple metal flow splitter (0.006 m ID). No external pump was used to pull the aerosol into the sampling line, the total flow (~ 3.0 lpm) in the sampling line (before the split) was due to the internal pump of all the instruments. The sample inlet positioning at the end of the wingspan also minimizes the influence of the aircraft propeller, located in the front of the cockpit.

### *2.2. Site description*

Pokhara Valley is Nepal's second largest populated valley (pop. >250,000) after the Kathmandu Valley (CBS, 2011). The valley is approximately at 815 m (a.s.l.), ~150 km west of the Kathmandu Valley, and ~90 km northeast of the southern plains (~100 m a.s.l.) bordering IGP. The valley is surrounded by mountains which are approximately 1000-2000 m (a.s.l.). Further north of the Pokhara Valley, within 30 km the elevation gradient increases rapidly to over 7000 m (a.s.l.) or higher (see Figure 1). This steep

elevation gradient is conducive for the orographic lift of humid air masses, and thus the valley also receives one of the highest rates of precipitation in Nepal and occasional strong convective updrafts leading to hailstorms and thunderstorms (Aryal et al., 2015). The mixing of dry westerly air masses with heated moist air masses from the Bay of Bengal produces strong convection over the Pokhara Valley, and thus results in strong updrafts. These strong convective activities are frequent in the pre-monsoon and monsoon season but do not occur during the winter season.

### *2.3. Test flight patterns over the Pokhara Valley*

Five test flights were conducted in the morning and evening period around Pokhara Valley (83.97° E, 28.19° N, 815 m a.s.l.) with each flight lasting for about 1 to 1.5 h from 5-7 May 2016. The flight pattern was consistently flown over the northwest part of the valley (Figure 1). A typical flight commenced from the Pokhara Regional Airport (818 m a.s.l.) and steadily flew 5-10 km northwest along the Pokhara Valley leaving the direct airport vicinity toward the Himalayas. This was followed by spirals up and down sampling from approximately 1000 to 4000 m, often reaching close to the lower base of the clouds in the free troposphere. Further climbs into the cloud layer were avoided during the test flights.

**Figure 1.** A typical test flight within the Pokhara Valley on 5 May 2016. The plot is generated using a Matlab-Google Earth toolbox (https://www.mathworks.com/matlabcentral/fileexchange/12954-google-earth-toolbox). Each dot is a single sample point (sampling frequency of 1Hz); the color of the dot indicates the total aerosol number concentration and the value of each color is shown as a color bar.

### *2.4. Data processing and quality*

The data from all the instruments was synced with the GPS clock, and the PC104 received all the data simultaneously and creates a common time-stamped data file. Prior to each test flight, a zero test was conducted to identify any possible leaks in the sample line.

The collected data from the five test flights went through multiple steps of quality control and quality assurance. Occasionally during the radio communication by the pilot with the ground station or air traffic controller, the CPC and the temperature sensor would record exceedingly high values. This noise is an interference picked up by the sensors from the 5 W radio transmission. The CPC and aethalometer is also sensitive to vibration in the aircraft, especially during upward and downward spiral motion, which may result in flow imbalance in these analyzers. This resulted in random noise segments for a few seconds in the data, which were flagged and not included in the analysis.

## 3. Results

### *3.1. General meteorology and air quality, aerosol properties in the Pokhara Valley*

#### 3.1.1. *Local and synoptic meteorology in the Pokhara Valley*

Climatologically, Pokhara Valley has a humid subtropical climate, characterized by a summer monsoon season from late June to September, preceded by a dry pre-monsoon (March-May, see Figure S2 in the supplement). Dominant winds in the valley are from the southeast and southwest with a strong diurnal variability in the wind speed (Aryal et al., 2015). On a local/regional, the winds in May 2016 were predominantly from the southeast with only occasional strong winds from the southwest (see Figure S3 in the supplement, using data available at the regional meteorological station at the Pokhara Airport). During the test flight period (5-7 May 2016), the wind was similar in directionality, with an hourly mean wind speed of 1.8 to 3.0 $ms^{-1}$, with low wind speed (<2.0 $ms^{-1}$) before noon, usually from the southeast, followed by stronger winds from the southwest and northwest (>2.4 $ms^{-1}$) which can continue until late night. The increased wind speed in the afternoon could be katabatic in nature as a result of differential heating of the mountain valley slopes and could be linked to pollution transport from surrounding regions (Gautam et al., 2011).

Three dominant synoptic meteorology regimes characterize the seasonality of South Asia (Lawrence and Lelieveld, 2010). They are summer (June-September), the winter monsoon (mid-November to February) and the monsoon-transition periods, which include the pre-monsoon season (March-May) and post-monsoon season (mid-September to mid-November). These synoptic regimes are also active in the Himalayas, including the Pokhara Valley. The monsoon transition period, during which the test flights were conducted, is characterized by westerlies over 20-30° N at 850 mb and above (see Figure 2). Figure 2 shows the daily wind vector over South Asia for 3, 5, 6 and 7 May 2016 generated using the NCEP NCAR Reanalysis data at 2.5°x 2.5° horizontal resolution. While the reanalysis data can be expected to represent the synoptic-scale phenomena in this region reasonably well, the rough terrain in the Himalayas presents a significant challenge for modeling and the data is thus likely to suffer from biases and other deviations from the observed meteorology (Xie et al., 2007). The wind vector at 850 mb in the 20-30° N latitude band was westerly with variable wind speeds in the IGP region near the Himalayan foothills. The wind direction varies diurnally at the 850 mb level, with the wind direction shifting to southwesterly near the Himalayan foothills. Westerlies were also generally prevalent at the 500 mb; however, in the mid-latitudes between 40-50° N (Central Asia) , a trough and crest-like feature of the westerlies moving from west to east Asia is visible (also observed by Lüthi et al., 2015), which was

also present prior to the study period. This wind feature was colder and more humid (see Figure S4 in the supplementary material) than the westerlies observed between 20-30° N. The meandering features (i.e., trough and crest) observed between 40-50° N affects the direction and magnitude of air masses (at 20-30° N) entering Nepal. For instance, the crest feature of the westerly was prevalent over the IGP and Nepal prior to 3 May, transitions into the trough feature after the 3$^{rd}$ and continues during the study period. The prevalence of the trough was characterized by the intrusion of wind into lower latitudes as well as into the IGP, also indicated by the change in the temperature and humidity (Figure S4). The intrusions of mid-latitude air masses also influence the westerlies entering Nepal in the 20-30° N sector (Lüthi et al., 2015). As discussed later, variations in the vertical profiles of aerosols above 3000 m (a.s.l.) could be associated with variations observed in these upper layer winds.

**Figure 2.** Daily wind vector data at 850 and 500 mb, plotted using the NCEP NCAR reanalysis (2.5° x 2.5°) data over South Asia from 1-7 May 2016. The colors indicate the wind speed in ms$^{-1}$. The plots were generated using the default setup at www.esrl.noaa.gov/psd/data/composites/day/.

### 3.1.2. Overview of the aerosol properties in the Pokhara Valley during the test flight period

The variation in aerosol loading (as reflected by AOD) reveals a strong seasonality in the Pokhara Valley (see supplementary figure S7 for a detailed description of aerosol properties in the Pokhara Valley during 2010-2016). The pre-monsoon season (also the time of the test flight) has the highest AOD values ($AOD_{500nm}$>0.6: Figure S7, S7a, S7a, and S5) followed by the monsoon low ($AOD_{500nm}$ ~0.2-0.3), most likely due to the wet removal of aerosols. AOD gradually increased (to ~0.4-0.5) during the post-monsoon through winter to the pre-monsoon season. Generally, the increase of total AOD (sum of fine and coarse) over the Pokhara Valley is dominated by fine-mode aerosol particles, except during the pre-monsoon and monsoon season, when a substantial fraction of coarse-mode particles were also present. The dominant aerosol in the Pokhara Valley is mostly *BC–like* (Giles et al., 2012), based on the values of absorption and extinction Ångstrom exponent (AAE and EAE at 440-870 nm); however, a substantial seasonal variation was observed from more mixed or dust-like in the pre-monsoon months, to more BC-like in the post-monsoon and winter months.

**Figure 3.** AOD and other data products from the Level1.5 AERONET direct product in the Pokhara Valley from 1-10 May 2016. The top panel includes AOD at 500nm and the AOD for coarse and fine modes (as shown in figure above as AOD-C, AOD-F). The bottom panel includes the Ångström Exponent (AE) for

440-870nm, the fine mode fraction and the visibility (km). The visibility data was available from the synoptic meteorology data available at http://www7.ncdc.noaa.gov/CDO/cdo

The aerosol optical properties (columnar) and synoptic meteorology are shown in Figure 3 and Figure S6 (in the supplementary). Prior to the flights days (1-4 May), higher AOD values were recorded in the Pokhara Valley (AOD>1) and dominated by a fine-mode fraction (~0.95). Hazy condition and low visibility (≤5 km) was recorded during the period in the valley (see Figure S6). Moving into the flight days, the AOD values decreased below 1, markedly by the drop in the fine-mode fraction and the improvement in haze condition and visibility. The flight day periods were also characterized by the presence of scattered clouds and thunderstorms (with no precipitation) in the afternoon, which also imply conditions for the strong vertical mixing of pollutants. It is indicative from Figure 3 and Figure S7 that the presence of high levels of pollution over the region from 1-4 May is followed by a short period of (relatively) cleaner conditions, which also coincides with the changes in the synoptic situation observed in the winds at 500 mb (described in section 3.1.1.)

### 3.2. Vertical profiles of absorbing aerosols, particle number and size distribution, temperature, and dew point

The five test flights are labeled as F1-5 in Figure 4, except F3 which is shown in the supplement (Fig. S10). F1 and F2 were conducted on 5 May, F3 and F4 on 6 May and F5 on 7 May 2016. Due to limitations of the flight permit, the test flights were conducted remaining within the Pokhara Valley as indicated by Figure 1. Among the five sampling flights, F1, F3, and F5 were morning flights, and F2 and F4 were afternoon flights (for details on sampling flights, see Table T1 in the supplement).

**Figure 4.** Vertical profiles of aerosol species and meteorological parameters during the 5-7 May 2016 test flights in the Pokhara Valley using the IKARUS microlight aircraft. The subplot in each row is arranged by (**i**) size distribution measured by the GRIMM OPS 1.108 (0.3-20 µm), limited to 1 µm in the figure, (**ii**) Total particle number concentration (also indicated as ***TPC***, Dp >14 nm) measured by the CPC 3760, along with absorbing aerosol mass density at 370 nm and 880 nm (**iii**) temperature (red line, in °C) and dew point (black dots, in °C) and relative humidity (or RH %), (**iv**) calculated absorption Ångstrom exponent averaged for every 500 meters elevation band. For the size distribution plot, the x-axis represents the optical diameter of the aerosol (nm), and the color bar represents the concentration ($10^x$ in $\#cm^{-3}$). Of the five test flights, only F1-2, F4-5 is shown here, F3 is in the supplementary. Number size distribution data from Flight F3 is not available due to the failure of the Grimm's pump during flight

initiation. In each subplot, the y-axis is the altitude above the mean sea level (in m). The origin of the y-axis is at 815 m (a.s.l.).

### 3.2.1. Diurnal variation in the vertical profiles

All the vertical aerosol profiles (Figure 3) showed a strong gradient below 2000 m (a.s.l.). Because of the valley geography, with surrounding mountains of about ~2000 m (a.s.l.) or higher, it is likely that the gradient observed below 2000 m (a.s.l.) could be related to emissions from the Pokhara Valley. The development (or dissolution) of the boundary layer during the day clearly influenced the evolution of the aerosol vertical profiles in the Pokhara Valley. The shallow boundary layer in the night, which continued till the morning, led to the accumulation of aerosols below 2000 m (a.s.l.) in the morning (see the morning flights (F1, F3, and F5) and a strong decrease with altitude was observed. For instance, in the morning profiles, the concentrations near the surface (<1000 m a.s.l.) for total particle number concentrations (also indicated as ***TPC*** in Figure 4) were mostly >$10^3$ $cm^{-3}$, but could reach ~ $3x10^4$ $cm^{-3}$ or higher (see F5 in Figure 4), which is attributed to the coupling of the shallow boundary layer and the emissions in the contained valley topography (Mues et al., 2017). Also, all the measured aerosol parameters (number size distribution for particles with diameters between 0.3 and 0.5 µm), the total particle concentration (>14 nm), and the absorption) vary similarly as a function of the altitude irrespective of the timing of the profiles. The similarity in the vertical concentration gradients of the absorbing aerosol mass concentrations and the aerosol number concentration above 2000 m (a.s.l.) provides evidence of similar emission sources or origins.

Within the morning profiles, substantial variations were observed; in F1 (5 May), in addition to the strong gradient below 2000 m (a.s.l.), there is a polluted layer above 3000 m (a.s.l.) which is not evident in F5. The BC concentration was close to 1 $\mu gm^{-3}$ up to 4000 m (a.s.l.) for F1 and stayed in that range until F5, where it dropped to about ~0.4 $\mu gm^{-3}$. The temperature and humidity profile also showed changes between the morning flights; the conditions during F1 are warmer (throughout the profile) and dryer (near the surface), compared to F5. This observed variation in the aerosol vertical profile (including the meteorology) may be indicative of cleaner atmospheric conditions (in terms of aerosol number and absorption) from 5 May to 7 May and could be associated with the arrival of colder airmasses in the Pokhara Valley. The near-surface BC concentrations measured in this study were much lower than surface BC concentrations measured in the pre-monsoon season (2013) in the Kathmandu Valley in the Himalayan foothills (hourly average: ~5-40 $\mu gm^{-3}$, Mues et al. (2017)), but comparable to winter measurements (2004) in Kanpur in the IGP (1-3 min average: ~1-7 $\mu gm^{-3}$, Tripathi et al. (2005)). In

Kanpur, Tripathi et al. (2005) observed BC concentrations close to 1 $\mu gm^{-3}$ up to 2000 m (a.s.l.) and a sharp gradient below 400 m (a.s.l.), most likely due to a shallow boundary layer in winter.

The elevated polluted air mass in F1 could be an indication of transport related to the mountain valley winds and/or synoptic transport related to the westerlies, common during this season (Gautam et al., 2011;Raatikainen et al., 2014;Marcq et al., 2010). Pre-monsoon airborne measurements over the IGP and near the Himalayan foothills during CALIPEX-2009 found a polluted aerosol layer (2-4x$10^3$ $cm^{-3}$ with a mean size of 0.13 µm diameter) below 4 km (a.s.l), attributed to biomass burning observed during this particular season (Padmakumari et al., 2013).

The afternoon profiles (F2: 5 May 2016 and F4: 6 May 2016) in contrast to the corresponding morning profile (F1 and F3) showed a more relatively mixed profile up to about 2500-3000 m, decreased then up to the maximum sampled altitude of just above 4000 m (a.s.l.). For instance, the concentrations of measured aerosol parameters up to 3000 m (a.s.l.) were comparable to the concentrations observed at ~1000 m (a.s.l.). Slight differences exist within the afternoon profiles, which may be related to local meteorology (boundary layer evolution) and mountain valley wind circulation in the afternoon. Cloud layers were present during the afternoon flights at and above 4000 m (a.s.l.) in F4 (also indicated by the sharp rise in RH from ca. 3600 m a.s.l.), which may have led to the scavenging of the aerosol by cloud droplets and thus explaining the observed decrease in the measured aerosol parameters.

### 3.2.2. Nature of absorbing aerosols in the Pokhara Valley

The absorption at multiple wavelengths was used to calculate the absorption Ångstrom exponent (AAE), shown in the right-most subplot in each row of Figure 4. AAE characterizes the wavelength (λ) dependence of absorption coefficient ($\text{Absorption coefficient or Abs. coeff} = K\lambda^{-AAE}$, Russell et al. (2010);Giles et al. (2012)). On a logarithmic scale, the above power relation between (Absorption coefficient and wavelength) is approximately a straight line (see supplementary S11 for an example case where both power and logarithmic form are plotted). The slope of the straight line is AAE. In our case, all the absorption coefficient measured between the 470 and 880 nm wavelength was used for the calculation of AAE. The mass absorption coefficients (MAC) of 14.5 and 7.77 $m^2 g^{-1}$, as prescribed by the manufacturer of the aethalometer (Hansen et al., 1984) for wavelength 470 nm and 880 nm, respectively were used to calculate the absorption coefficient (the unit for the absorption coefficient is $m^{-1}$). The calculated AAE was averaged for each 100 m (a.s.l.), as shown in the figure. The sampling resolution for the aethalometer is 2 min (see Table 1), which resulted in no (in a few cases) or few data

(after flagging) if smaller height bins were chosen. The AAE profile differed markedly between the morning (F1, F3, and F5) and afternoon (F2 and F4) profiles, with morning profiles showed large variations along the height. Surface AAE (~1000 m a.s.l.) was close to 0.8 to 1.2 for all the flights which indicate the presence of BC from a mix of sources (biomass burning and fossil fuel combustion. A source-diagnostic analysis of C-isotopes of elemental carbon (EC) in TSP (total suspended particulates) collected in Pokhara during April 2013-March 2014 showed that the biomass burning and fossil fuel combustion contributes nearly 50 % each to the (annual average) EC concentration (Li et al., 2016). The AAE values above surface (>1000 m a.s.l.) varied from 0.5 to 2, but mostly fell into the range of 0.9- 1.2, which is typically reported for mixed to *BC like* aerosols from urban and industrial emissions (Russell et al., 2010;Yang et al., 2009;Dumka et al., 2014). AAE<1 could also be indicative of a composite aerosol, where a BC aerosol (or "core") is coated with absorbing or non-absorbing aerosols (Gyawali et al., 2009).

**Figure 5**. Aerosol extinction coefficient (at 532 nm) vertical profile (left) and aerosol type classification based on the CALIPSO level 2 retrieval (right). Only the CALIPSO overpass over the Pokhara Valley or nearby locations (such as Kathmandu Valley region, and the region to the west of Pokhara Valley) is included. The extinction profile is averaged for the region 27-28.5° N latitude, which also includes the Pokhara Valley.

### 3.2.3. Comparison of the satellite-derived vertical profiles with measurements

The measured vertical profiles were also complemented with CALIPSO retrievals over the Pokhara Valley (Figure 5). Level 2 (version 4), cloud and quality screened data were used to generate the vertically resolved extinction (at 532 nm) and aerosol classification. The CALIPSO satellite had only three overpasses over the Pokhara Valley between 1 and 10 May 2016 (the extinction profile lines with circle markers are for the Pokhara Valley). Therefore, the satellite overpasses through nearby regions such as the Kathmandu Valley region to the east and the region to the west of the Pokhara Valley (denoted by *WestPV* in Figure 5) were also considered. The range of extinction values for the Pokhara Valley (0.15-0.25 $km^{-1}$ especially around 2000-4000 m a.s.l.) were similar to pre-monsoon values (0.15-3 $km^{-1}$) reported in Nainital (a hilly station located ~2000 m (a.s.l.) in India, and 400 km west of the Pokhara Valley) and slightly less than Kanpur, a site in the IGP, about 400 km to the southwest of Pokhara (Dumka et al., 2014). A large extinction (>0.5 $km^{-1}$ ) was observed on 1 May 2016 over the Pokhara Valley at an altitude of 3-4 km (a.s.l.) which can be attributed to smoke (biomass- related) and polluted dust (a mixture of dust and biomass smoke or urban pollution) as evident by the aerosol type

classification. Aerosols over the IGP and in the proximity of the Himalayan foothills were mainly "Dust" on 1 May 2016. Although not conclusive, the 9 May aerosol type classification is markedly different from 1 May with the absence of dust in the IGP, and absence of polluted dust or smoke over the Pokhara Valley.

**Figure 6**. HYSPLIT (Hybrid Single Particle Lagrangian Integrated Trajectory, Draxler and Hess (1998)) 3 day back trajectories of air masses arriving at 3 different heights (800 m, 1500 m and 2500 m) from above the ground level (AGL~ 815 m a.s.l.) in the Pokhara Valley (28.19° N, 83.98° E) during 5-7 May 2016. NCEP GDAS (Global Data Assimilation System) Reanalysis data with 1°x1° horizontal resolution were used as the input meteorology. The trajectory data is overlayed with the active fire data (extracted from the MODIS collection 6 database, available at https://firms2.modaps.eosdis.nasa.gov/active_fire. Each green dot with a gray edge is an active fire, and the strength of the active fire is indicated by the "*frp" value,* which is the fire radiative power in megawatts.

3.2.4. Role of synoptic circulation in modulating aerosol properties over the Pokhara Valley

The measured vertical profiles and available satellite data from MODIS (See Figure S8) and CALIPSO suggest that the synoptic-scale circulation were changing during the study period. The changing synoptic circulation also influenced the transport of polluted air into the Pokhara Valley. The regional meteorology station in the Pokhara Valley reported hazy conditions till 5 May 2016(see Figure S6) which disappeared from 6 May 2016 onwards followed by clear days with scattered clouds during the daytime and thunderstorms in the afternoon. The variation in the AOD, AOD-F and Fine Mode Fraction (FMF) from AERONET (only level 1.5 data were available, see Figure S7) also showed that high turbidity in the atmospheric column, dominated by fine-mode aerosols before 5 May 2016 ($AOD_{500nm}$>2.0, FMF >0.9), which declined sharply after 5 May 2016. The variation in the horizontal visibility (or visual range) measured at the meteorology station in the Pokhara Valley further indicates that the intensity of pollution declined during the study period, especially starting on 5 May 2016.

Three day back trajectories (72 h) were generated using HYSPLIT (Hybrid Single Particle Lagrangian Integrated Trajectory) for air masses arriving in the Pokhara Valley at 800 m, 1,500 m and 2,500 m from above ground level (AGL) for the test flight period (see Figure 6). The NCEP GDAS reanalysis data with a 1°x1° horizontal resolution were used as the input meteorology for the trajectories. The majority of air masses (especially at 1500 and 2000 m AGL) were westerly. A high resolution (0.0625° horizontal)

simulation of air mass trajectories during the pre-monsoon period over the Himalayas and Tibetan Plateau region by Lüthi et al. (2015) also identified synoptic-scale transport (as westerly advection around 500 mb) and a convection-enabled polluted airmass from the IGP as a major mechanism of transport of air pollution in the Himalayas. Transport of air pollution by both mechanisms was coupled with the diurnal expansion of PBL height in the IGP where the trajectory height was similar to planetary boundary layer (PBL) height thus allowing mixing up of the polluted layer, also observed by Raatikainen et al. (2014) over Gual Pahari (IGP site) and Mukteswor (Himalayan foothill site).

During the study period, the direction of the trajectories varied as the air masses entered Nepal and eventually into the Pokhara Valley. On 5 and 6 May 2016, the air masses (at 1500 and 2000 m AGL) were mostly northwesterly traversing through northern India and western Nepal before entering the Pokhara Valley. A shift in the trajectory direction from north westerly to south westerly was observed on 7 May 2016, where the trajectories were moving through central India and the southern foothills into the Pokhara Valley. The observed shift in the trajectories at 1500 and 2500 m AGL was modulated by the synoptic-scale changes in the mid-latitude (over Central Asia) air masses (40-50° N) (Lüthi et al., 2015). The intrusion (in the form of a trough) of the cold and humid air masses from 40-50° N (see Figure 2) into 20-30° N occurred during the study period. As the trough moves eastward, it shifts the synoptic air mass at 20-30° N from northwesterly to southwesterly on 7 May 2016. The elevated polluted layer on 5 and 6 May 2016 (Figure 4) could be the result of this modulation of the westerly. The northwesterly airmass entered Nepal via Northern India, where MODIS retrievals showed a high aerosol loading (See Figure S8), which could be mainly attributed to the numerous biomass fire events (See Figure S9) observed in North India. In addition, numerous forest fires were also reported in western Nepal during the same period. However, the absorption signal from the flight measurement does not clearly show higher absorption at shorter wavelengths compared to absorption at 880 or longer wavelengths. This also implies that the observed elevated polluted layer in the Pokhara Valley is not entirely due to the biomass burning plume intercepted by the westerlies or north-westerlies. As the airmass origin shifts to southwesterly on 7 May 2016 (detected during flight F5), the synoptic air mass bypassed the high AOD loading over north India and contained the cold and relatively clean air from Central Asia. This resulted in the disappearance of the polluted layer over 2000 m (a.s.l.) during flight F5.

## *4.* Conclusion

This paper provides an overview of the pre-monsoon airborne measurement carried out with a microlight aircraft platform in the Pokhara Valley in Nepal, the first-of-their-kind airborne aerosol

446 measurements in the Himalayan foothill region. The objective of the overall airborne campaign in the
447 Himalayan region was to quantify the vertical distribution of aerosols over a polluted mountain valley
448 region, as well as to measure the extent of regional transport into the Himalayas. In this paper,
449 measurements from the test flights during May 2016 are summarized. These mainly include vertical
450 profiles of aerosol number and size distribution, multi-wavelength aerosol absorption, black carbon,
451 total particle concentration, and meteorological variables. The instrument package, designed for a
452 microlight sampling was fitted to an IKARUS-C42 microlight aircraft. A total of five test flights were
453 conducted between 5 and 7 May 2016, including morning and evening flights for about 1-1.5 h each, as
454 well as vertical spirals to characterize vertical profiles of aerosols and meteorological parameters

455 The results presented in this paper should be considered as a pilot study mapping out the
456 aerosol concentrations and their interactions with meteorological processes in the Pokhara Valley due
457 to the limited flight time. In all the measured flights, the vertical profiles of aerosol parameters showed
458 strong gradients along the atmospheric column. The observed total number concentration gradient was
459 strongly influenced by the mountain valley boundary layer, which resulted in a sharp gradient below
460 about 1500-2000 m (a.s.l.). The increase of boundary layer height contributed to the differences in the
461 morning and afternoon profiles. Similar vertical profiles of BC concentrations and aerosol total particle
462 number concentrations provided evidence of common emission sources or co-located origins. The
463 observed BC concentration near the surface (~ 1000 m a.s.l.) was much lower than pre-monsoon BC
464 concentrations measured in the Kathmandu Valley but comparable to values reported during the winter
465 season in Kanpur in the IGP. The AAE estimates near the surface, based on the absorption value, fell in
466 the range of 0.9-1.2, which indicates the presence of *BC like* and mixed (dust, urban, biomass) aerosols.
467 An elevated polluted layer was observed at around 3 km (a.s.l.) over the Pokhara Valley during this
468 study. Characterized by a strong presence of dust in the IGP and polluted continental airmasses over the
469 Pokhara Valley, the polluted layer could be linked with the westerly synoptic circulations and regional
470 transport from the IGP and surrounding regions. The direction of the synoptic transport entering the
471 Himalayan foothills and into Pokhara Valley, however, was influenced by the Westerlies at mid-latitudes
472 (40-50° N). The extent of transport can be better quantified with regional airborne measurements along
473 the south-north transect through the region between the IGP and the Himalayan foothills at high
474 altitudes in the Himalayas, including the Pokhara Valley. We will explore the extent of such regional
475 transport in a subsequent publication that will be primarily based on the airborne measurements in
476 phase II (December 2016- January 2017) in the Pokhara Valley and in the surrounding region. The

subsequent paper will also characterize the extent of vertical transport from three different mountain valleys located at different elevations along the south-north transect.

*Acknowledgments.* The authors would like to thank the Ministry of Population and Environment, Nepal (www.mope.gov.np), and the Civil Aviation Authority of Nepal (https://www.caanepal.org.np) for approving this campaign in Nepal. We are grateful for funding for IASS and for this study from the German Federal Ministry for Education and Research (BMBF) and the Brandenburg Ministry for Science, Research and Culture (MWFK). We would also like to thank the NASA DAACs for the data repository of MODIS, and CALIPSO satellite and as well as NOAA for the meteorology data. Special thanks to the NASA AERONET team especially Gupta Giri for operating and maintaining the Pokhara station. The work was only possible by the support and team-work of the Pokhara Ultralight Company and their operational staff for the aircraft and air traffic management.

## *5.* References

Aryal, D., Rosoff, Y. N., and Devkota, L. P.: A Severe Hailstorm at Pokhara: CAPE Stability Index Calculations, Journal of Geosciences and Geomatics, 3, 142-153, 2015.

Bollasina, M. A., Ming, Y., and Ramaswamy, V.: Anthropogenic Aerosols and the Weakening of the South Asian Summer Monsoon, Science, 334, 502-505, 10.1126/science.1204994, 2011.

Brauer, M., Amann, M., Burnett, R. T., Cohen, A., Dentener, F., Ezzati, M., Henderson, S. B., Krzyzanowski, M., Martin, R. V., Van Dingenen, R., van Donkelaar, A., and Thurston, G. D.: Exposure assessment for estimation of the global burden of disease attributable to outdoor air pollution, Environmental science & technology, 46, 652-660, 10.1021/es2025752, 2012.

Burney, J., and Ramanathan, V.: Recent climate and air pollution impacts on Indian agriculture, Proceedings of the National Academy of Sciences, 111, 16319-16324, 10.1073/pnas.1317275111, 2014.

Cho, C., Kim, S. W., Rupakheti, M., Park, J. S., Panday, A., Yoon, S. C., Kim, J. H., Kim, H., Jeon, H., Sung, M., Kim, B. M., Hong, S. K., Park, R. J., Rupakheti, D., Mahata, K. S., Praveen, P. S., Lawrence, M. G., and Holben, B.: Wintertime aerosol optical and radiative properties in the Kathmandu Valley during the SusKat-ABC field campaign, Atmos. Chem. Phys., 17, 12617-12632, 10.5194/acp-17-12617-2017, 2017.

Cong, Z., Kawamura, K., Kang, S., and Fu, P.: Penetration of biomass-burning emissions from South Asia through the Himalayas: new insights from atmospheric organic acids, 5, 9580, 10.1038/srep09580 http://dharmasastra.live.cf.private.springer.com/articles/srep09580#supplementary-information, 2015.

Decesari, S., Facchini, M. C., Carbone, C., Giulianelli, L., Rinaldi, M., Finessi, E., Fuzzi, S., Marinoni, A., Cristofanelli, P., Duchi, R., Bonasoni, P., Vuillermoz, E., Cozic, J., Jaffrezo, J. L., and Laj, P.: Chemical composition of PM<sub>10</sub> and PM<sub>1</sub> at the high-altitude Himalayan station Nepal Climate Observatory-Pyramid (NCO-P) (5079 m a.s.l.), Atmos. Chem. Phys., 10, 4583-4596, 10.5194/acp-10-4583-2010, 2010.

Dey, S., and Di Girolamo, L.: A climatology of aerosol optical and microphysical properties over the Indian subcontinent from 9 years (2000–2008) of Multiangle Imaging Spectroradiometer (MISR) data, Journal of Geophysical Research: Atmospheres, 115, n/a-n/a, 10.1029/2009JD013395, 2010.

Draxler, R. R., and Hess, G. D.: An overview of the HYSPLIT_4 modeling system for trajectories, dispersion, and deposition, Aust. Meteor. Mag, 47, 295–230, 1998.

Dumka, U. C., N. Tripathi, S., Misra, A., Giles, D. M., Eck, T. F., Sagar, R., and Holben, B. N.: Latitudinal variation of aerosol properties from Indo-Gangetic Plain to central Himalayan foothills during TIGERZ campaign, Journal of Geophysical Research: Atmospheres, 119, 4750-4769, 10.1002/2013jd021040, 2014.

Gautam, R., Hsu, N. C., Lau, K. M., and Kafatos, M.: Aerosol and rainfall variability over the Indian monsoon region: distributions, trends and coupling, Ann. Geophys., 27, 3691-3703, 10.5194/angeo-27-3691-2009, 2009a.

Gautam, R., Hsu, N. C., Lau, K. M., Tsay, S. C., and Kafatos, M.: Enhanced pre-monsoon warming over the Himalayan-Gangetic region from 1979 to 2007, Geophysical Research Letters, 36, n/a-n/a, 10.1029/2009GL037641, 2009b.

Gautam, R., Hsu, N. C., Tsay, S. C., Lau, K. M., Holben, B., Bell, S., Smirnov, A., Li, C., Hansell, R., Ji, Q., Payra, S., Aryal, D., Kayastha, R., and Kim, K. M.: Accumulation of aerosols over the Indo-Gangetic plains and southern slopes of the Himalayas: distribution, properties and radiative effects during the 2009 pre-monsoon season, Atmospheric Chemistry and Physics, 11, 12841-12863, 10.5194/acp-11-12841-2011, 2011.

Giles, D. M., Holben, B. N., Eck, T. F., Sinyuk, A., Smirnov, A., Slutsker, I., Dickerson, R. R., Thompson, A. M., and Schafer, J. S.: An analysis of AERONET aerosol absorption properties and classifications representative of aerosol source regions, Journal of Geophysical Research: Atmospheres, 117, n/a-n/a, 10.1029/2012jd018127, 2012.

Gogoi, M. M., Moorthy, K. K., Kompalli, S. K., Chaubey, J. P., Babu, S. S., Manoj, M. R., Nair, V. S., and Prabhu, T. P.: Physical and optical properties of aerosols in a free tropospheric environment: Results from long-term observations over western trans-Himalayas, Atmospheric Environment, 84, 262-274, https://doi.org/10.1016/j.atmosenv.2013.11.029, 2014.

Guttikunda, S. K., Goel, R., and Pant, P.: Nature of air pollution, emission sources, and management in the Indian cities, Atmospheric Environment, 95, 501-510, http://dx.doi.org/10.1016/j.atmosenv.2014.07.006, 2014.

Gyawali, M., Arnott, W. P., Lewis, K., and Moosmüller, H.: In situ aerosol optics in Reno, NV, USA during and after the summer 2008 California wildfires and the influence of absorbing and non-absorbing organic coatings on spectral light absorption, Atmos. Chem. Phys., 9, 8007-8015, 10.5194/acp-9-8007-2009, 2009.

Hansen, A. D. A., Rosen, H., and Novakov, T.: The aethalometer — An instrument for the real-time measurement of optical absorption by aerosol particles, Science of The Total Environment, 36, 191-196, https://doi.org/10.1016/0048-9697(84)90265-1, 1984.

Jai Devi, J., Tripathi, S. N., Gupta, T., Singh, B. N., Gopalakrishnan, V., and Dey, S.: Observation-based 3-D view of aerosol radiative properties over Indian Continental Tropical Convergence Zone: implications to regional climate, Tellus B, 63, 971-989, 10.1111/j.1600-0889.2011.00580.x, 2011.

Junkermann, W.: An Ultralight Aircraft as Platform for Research in the Lower Troposphere: System Performance and First Results from Radiation Transfer Studies in Stratiform Aerosol Layers and Broken Cloud Conditions, Journal of Atmospheric and Oceanic Technology, 18, 934-946, 10.1175/1520-0426(2001)018<0934:auaapf>2.0.co;2, 2001.

Kaskaoutis, D. G., Singh, R. P., Gautam, R., Sharma, M., Kosmopoulos, P. G., and Tripathi, S. N.: Variability and trends of aerosol properties over Kanpur, northern India using AERONET data (2001–10), Environmental Research Letters, 7, 024003, 10.1088/1748-9326/7/2/024003, 2012.

Kuhlmann, J., and Quaas, J.: How can aerosols affect the Asian summer monsoon? Assessment during three consecutive pre-monsoon seasons from CALIPSO satellite data, Atmos. Chem. Phys., 10, 4673-4688, 10.5194/acp-10-4673-2010, 2010.

Lau, W.: Atmospheric science: Desert dust and monsoon rain, Nature Geosci, 7, 255-256, 10.1038/ngeo2115, 2014.

564 Lawrence, M. G., and Lelieveld, J.: Atmospheric pollutant outflow from southern Asia: a review, Atmos.
565 Chem. Phys., 10, 11017-11096, 10.5194/acp-10-11017-2010, 2010.
566 Li, C., Bosch, C., Kang, S., Andersson, A., Chen, P., Zhang, Q., Cong, Z., Chen, B., Qin, D., and Gustafsson,
567 O.: Sources of black carbon to the Himalayan-Tibetan Plateau glaciers, Nat Commun, 7, 12574,
568 10.1038/ncomms12574, 2016.
569 Lüthi, Z. L., Škerlak, B., Kim, S. W., Lauer, A., Mues, A., Rupakheti, M., and Kang, S.: Atmospheric brown
570 clouds reach the Tibetan Plateau by crossing the Himalayas, Atmos. Chem. Phys., 15, 6007-6021,
571 10.5194/acp-15-6007-2015, 2015.
572 Marcq, S., Laj, P., Roger, J. C., Villani, P., Sellegri, K., Bonasoni, P., Marinoni, A., Cristofanelli, P., Verza, G.
573 P., and Bergin, M.: Aerosol optical properties and radiative forcing in the high Himalaya based on
574 measurements at the Nepal Climate Observatory-Pyramid site (5079 m a.s.l.), Atmos. Chem. Phys., 10,
575 5859-5872, 10.5194/acp-10-5859-2010, 2010.
576 Marinoni, A., Cristofanelli, P., Laj, P., Duchi, R., Putero, D., Calzolari, F., Landi, T. C., Vuillermoz, E.,
577 Maione, M., and Bonasoni, P.: High black carbon and ozone concentrations during pollution transport in
578 the Himalayas: Five years of continuous observations at NCO-P global GAW station, Journal of
579 Environmental Sciences, 25, 1618-1625, http://dx.doi.org/10.1016/S1001-0742(12)60242-3, 2013.
580 Mues, A., Rupakheti, M., Münkel, C., Lauer, A., Bozem, H., Hoor, P., Butler, T., and Lawrence, M. G.:
581 Investigation of the mixing layer height derived from ceilometer measurements in the Kathmandu Valley
582 and implications for local air quality, Atmos. Chem. Phys., 17, 8157-8176, 10.5194/acp-17-8157-2017,
583 2017.
584 Neitola, K., Asmi, E., Komppula, M., Hyvärinen, A. P., Raatikainen, T., Panwar, T. S., Sharma, V. P., and
585 Lihavainen, H.: New particle formation infrequently observed in Himalayan foothills – why?, Atmos.
586 Chem. Phys., 11, 8447-8458, 10.5194/acp-11-8447-2011, 2011.
587 Padmakumari, B., Maheskumar, R. S., Morwal, S. B., Harikishan, G., Konwar, M., Kulkarni, J. R., and
588 Goswami, B. N.: Aircraft observations of elevated pollution layers near the foothills of the Himalayas
589 during CAIPEEX-2009, Quarterly Journal of the Royal Meteorological Society, 139, 625-638,
590 10.1002/qj.1989, 2013.
591 Panday, A. K., and Prinn, R. G.: Diurnal cycle of air pollution in the Kathmandu Valley, Nepal:
592 Observations, Journal of Geophysical Research: Atmospheres, 114, D09305, 10.1029/2008JD009777,
593 2009.
594 Pandey, S. K., Vinoj, V., Landu, K., and Babu, S. S.: Declining pre-monsoon dust loading over South Asia:
595 Signature of a changing regional climate, Scientific Reports, 7, 16062, 10.1038/s41598-017-16338-w,
596 2017.
597 Putero, D., Landi, T. C., Cristofanelli, P., Marinoni, A., Laj, P., Duchi, R., Calzolari, F., Verza, G. P., and
598 Bonasoni, P.: Influence of open vegetation fires on black carbon and ozone variability in the southern
599 Himalayas (NCO-P, 5079 m a.s.l.), Environ Pollut, 184, 597-604, 10.1016/j.envpol.2013.09.035, 2014.
600 Putero, D., Cristofanelli, P., Marinoni, A., Adhikary, B., Duchi, R., Shrestha, S. D., Verza, G. P., Landi, T. C.,
601 Calzolari, F., Busetto, M., Agrillo, G., Biancofiore, F., Di Carlo, P., Panday, A. K., Rupakheti, M., and
602 Bonasoni, P.: Seasonal variation of ozone and black carbon observed at Paknajol, an urban site in the
603 Kathmandu Valley, Nepal, Atmos. Chem. Phys., 15, 13957-13971, 10.5194/acp-15-13957-2015, 2015.
604 Raatikainen, T., Hyvärinen, A. P., Hatakka, J., Panwar, T. S., Hooda, R. K., Sharma, V. P., and Lihavainen,
605 H.: The effect of boundary layer dynamics on aerosol properties at the Indo-Gangetic plains and at the
606 foothills of the Himalayas, Atmospheric Environment, 89, 548-555, 10.1016/j.atmosenv.2014.02.058,
607 2014.
608 Ramana, M. V., Ramanathan, V., Podgorny, I. A., Pradhan, B. B., and Shrestha, B.: The direct
609 observations of large aerosol radiative forcing in the Himalayan region, Geophysical Research Letters,
610 31, n/a-n/a, 10.1029/2003GL018824, 2004.

611 Ramanathan, V., Crutzen, P. J., Kiehl, J. T., and Rosenfeld, D.: Aerosols, Climate, and the Hydrological
612 Cycle, Science, 294, 2119-2124, 10.1126/science.1064034, 2001.
613 Russell, P. B., Bergstrom, R. W., Shinozuka, Y., Clarke, A. D., DeCarlo, P. F., Jimenez, J. L., Livingston, J. M.,
614 Redemann, J., Dubovik, O., and Strawa, A.: Absorption Angstrom Exponent in AERONET and related data
615 as an indicator of aerosol composition, Atmos. Chem. Phys., 10, 1155-1169, 10.5194/acp-10-1155-2010,
616 2010.
617 Shrestha, P., Barros, A. P., and Khlystov, A.: Chemical composition and aerosol size distribution of the
618 middle mountain range in the Nepal Himalayas during the 2009 pre-monsoon season, Atmospheric
619 Chemistry and Physics, 10, 11605-11621, 2010.
620 Shrestha, P., Barros, A. P., and Khlystov, A.: CCN estimates from bulk hygroscopic growth factors of
621 ambient aerosols during the pre-monsoon season over Central Nepal, Atmospheric Environment, 67,
622 120-129, http://dx.doi.org/10.1016/j.atmosenv.2012.10.042, 2013.
623 Stone, E. A., Schauer, J. J., Pradhan, B. B., Dangol, P. M., Habib, G., Venkataraman, C., and Ramanathan,
624 V.: Characterization of emissions from South Asian biofuels and application to source apportionment of
625 carbonaceous aerosol in the Himalayas, Journal of Geophysical Research: Atmospheres, 115, n/a-n/a,
626 10.1029/2009JD011881, 2010.
627 Tripathi, S. N., Dey, S., Tare, V., Satheesh, S. K., Lal, S., and Venkataramani, S.: Enhanced layer of black
628 carbon in a north Indian industrial city, Geophysical Research Letters, 32, n/a-n/a,
629 10.1029/2005gl022564, 2005.
630 Venkataraman, C., Habib, G., Kadamba, D., Shrivastava, M., Leon, J. F., Crouzille, B., Boucher, O., and
631 Streets, D. G.: Emissions from open biomass burning in India: Integrating the inventory approach with
632 high-resolution Moderate Resolution Imaging Spectroradiometer (MODIS) active-fire and land cover
633 data, Global Biogeochemical Cycles, 20, n/a-n/a, 10.1029/2005GB002547, 2006.
634 Venzac, H., Sellegri, K., Laj, P., Villani, P., Bonasoni, P., Marinoni, A., Cristofanelli, P., Calzolari, F., Fuzzi,
635 S., Decesari, S., Facchini, M. C., Vuillermoz, E., and Verza, G. P.: High frequency new particle formation in
636 the Himalayas, Proc Natl Acad Sci U S A, 105, 15666-15671, 10.1073/pnas.0801355105, 2008.
637 Vinoj, V., Rasch, P. J., Wang, H., Yoon, J.-H., Ma, P.-L., Landu, K., and Singh, B.: Short-term modulation of
638 Indian summer monsoon rainfall by West Asian dust, Nature Geosci, 7, 308-313, 10.1038/ngeo2107

639 http://www.nature.com/ngeo/journal/v7/n4/abs/ngeo2107.html#supplementary-information, 2014.
640 Xie, A., Ren, J., Qin, X., and Kang, S.: Reliability of NCEP/NCAR reanalysis data in the Himalayas/Tibetan
641 Plateau, Journal of Geographical Sciences, 17, 421-430, 10.1007/s11442-007-0421-2, 2007.
642 Yang, M., Howell, S. G., Zhuang, J., and Huebert, B. J.: Attribution of aerosol light absorption to black
643 carbon, brown carbon, and dust in China – interpretations of atmospheric measurements during EAST-
644 AIRE, Atmos. Chem. Phys., 9, 2035-2050, 10.5194/acp-9-2035-2009, 2009.

645

646

647 **List of Tables**

648 Table 1. Instrument package deployed in the microlight aircraft

| Parameters | Instruments | Method | Sampling time resolution |
|---|---|---|---|
| 1. Aerosol particle number size distribution (0.3 - 20 µm) | GRIMM 1.108 | Light scattering | 6 s |
| **2.** Total particle number concentration (>14 nm) | TSI CPC 3760 | Condensation/light scattering | 1 s |
| 3. Aerosol spectral absorption | Magee AE42 | 7 wavelengths, light attenuation | 2 min |
| 4. Dew point sensor | METEOLABOR, TPS3 | Chilled Mirror | 1 Hz |
| 5. Temperature | Thermocouple | - | 1 Hz |
| 6. Data acquisition system | PC 104+ GPS | --- | --- |
| 7. Power supply | Aircraft battery pack, $LiFEPO_4$ battery | 12 V, >15 AH | |

649

## List of Figures

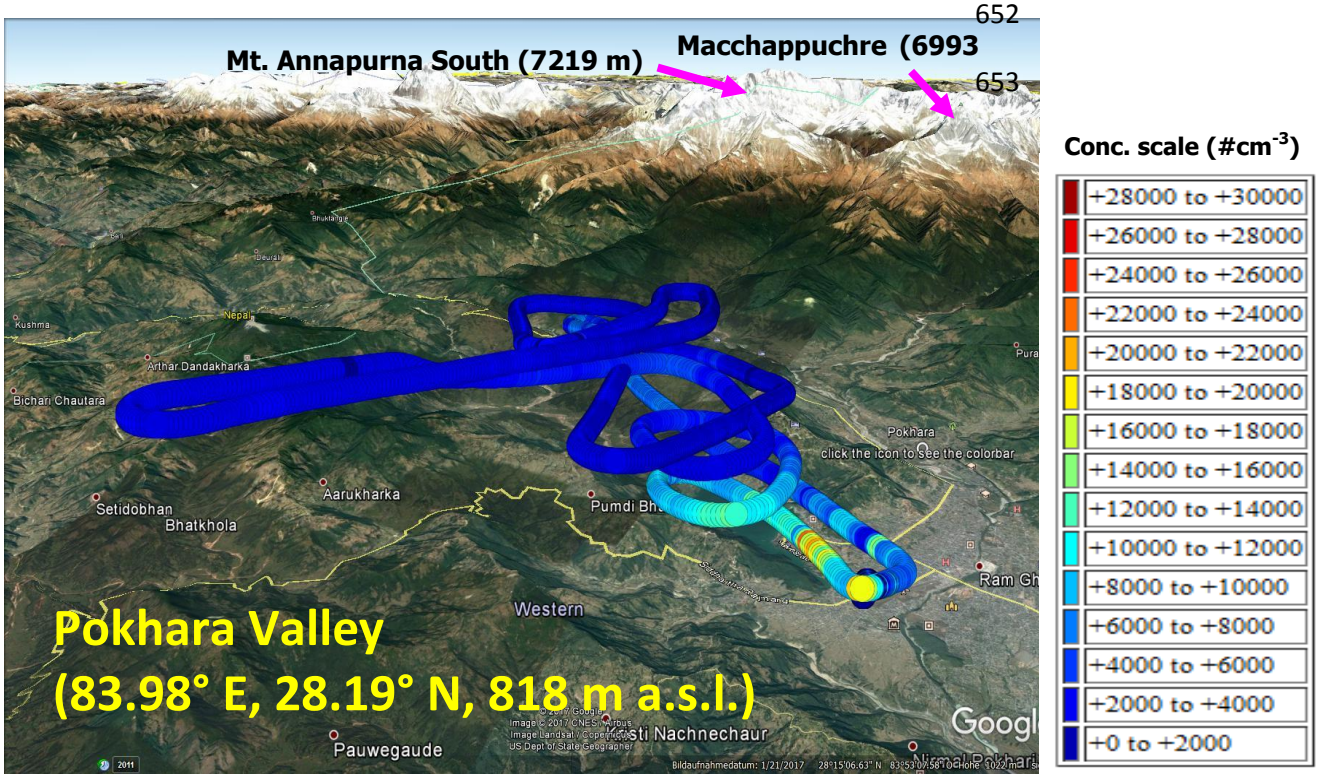


**Figure 1.** A typical test flight within the Pokhara Valley on 5 May 2016. The plot is generated using a Matlab-Google Earth toolbox (https://www.mathworks.com/matlabcentral/fileexchange/12954-google-earth-toolbox). Each dot is a single sample point (sampling frequency of 1Hz) and the color of the dot indicates the total aerosol number concentration (in # $cm^{-3}$) and the value of each color is shown as a color bar.

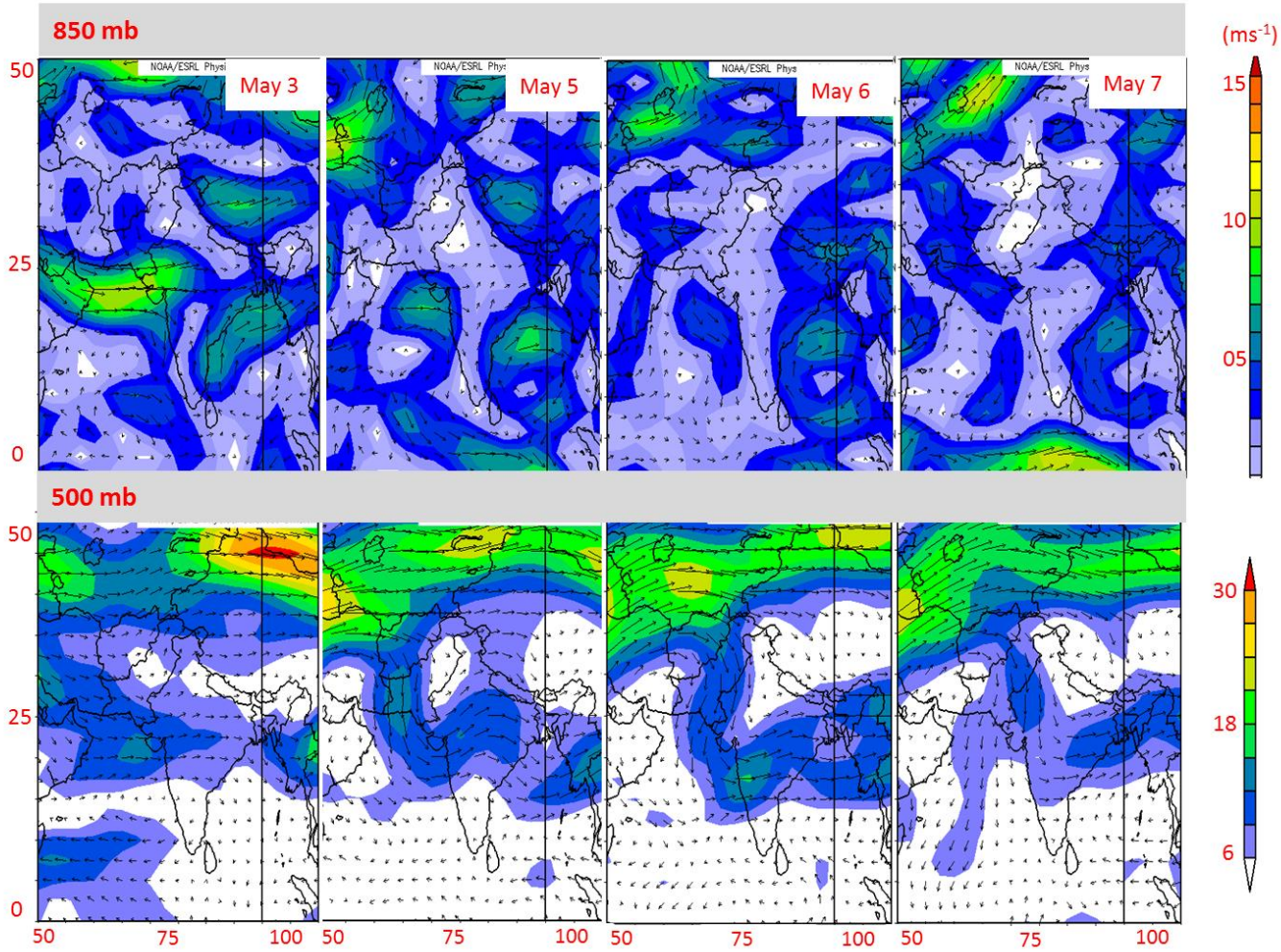


**Figure 2.** Daily wind vector data at 850 and 500 mb plotted using the NCEP NCAR reanalysis (2.5° x 2.5°) data over South Asia from 1-7 May 2016. The colors indicate the wind speed in $ms^{-1}$. The plots were generated using the default set-up at www.esrl.noaa.gov/psd/data/composites/day/.

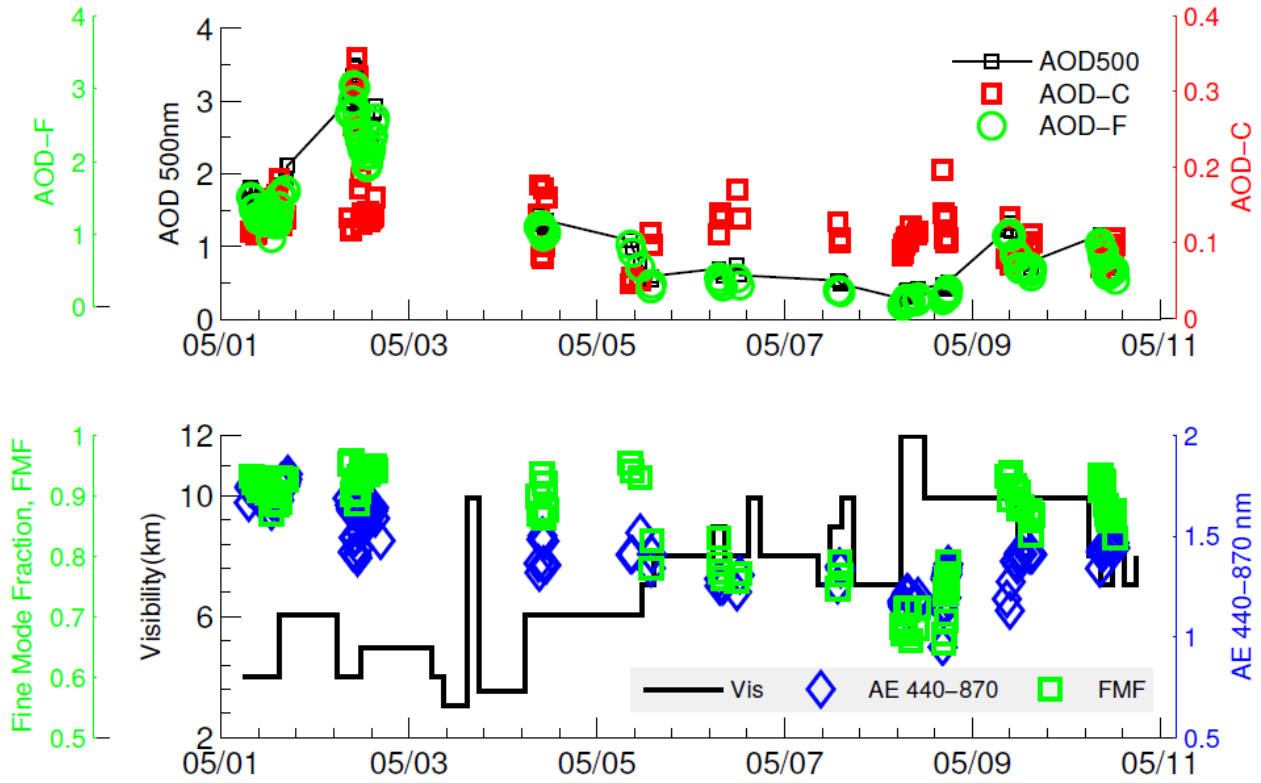


665

666 **Figure 3.** AOD and other data products from the Level1.5 AERONET direct product in the Pokhara Valley from 1-10 May 2016. The top panel
667 includes AOD at 500nm and AOD coarse and fine (as shown in figure above as AOD-C, AOD-F). The bottom panel includes ångström Exponent
668 (AE) 440-870nm, fine mode fraction and visibility (km). The visibility data was available from the synoptic meteorology data available at the
669 http://www7.ncdc.noaa.gov/CDO/cdo/

670

**Figure 4**

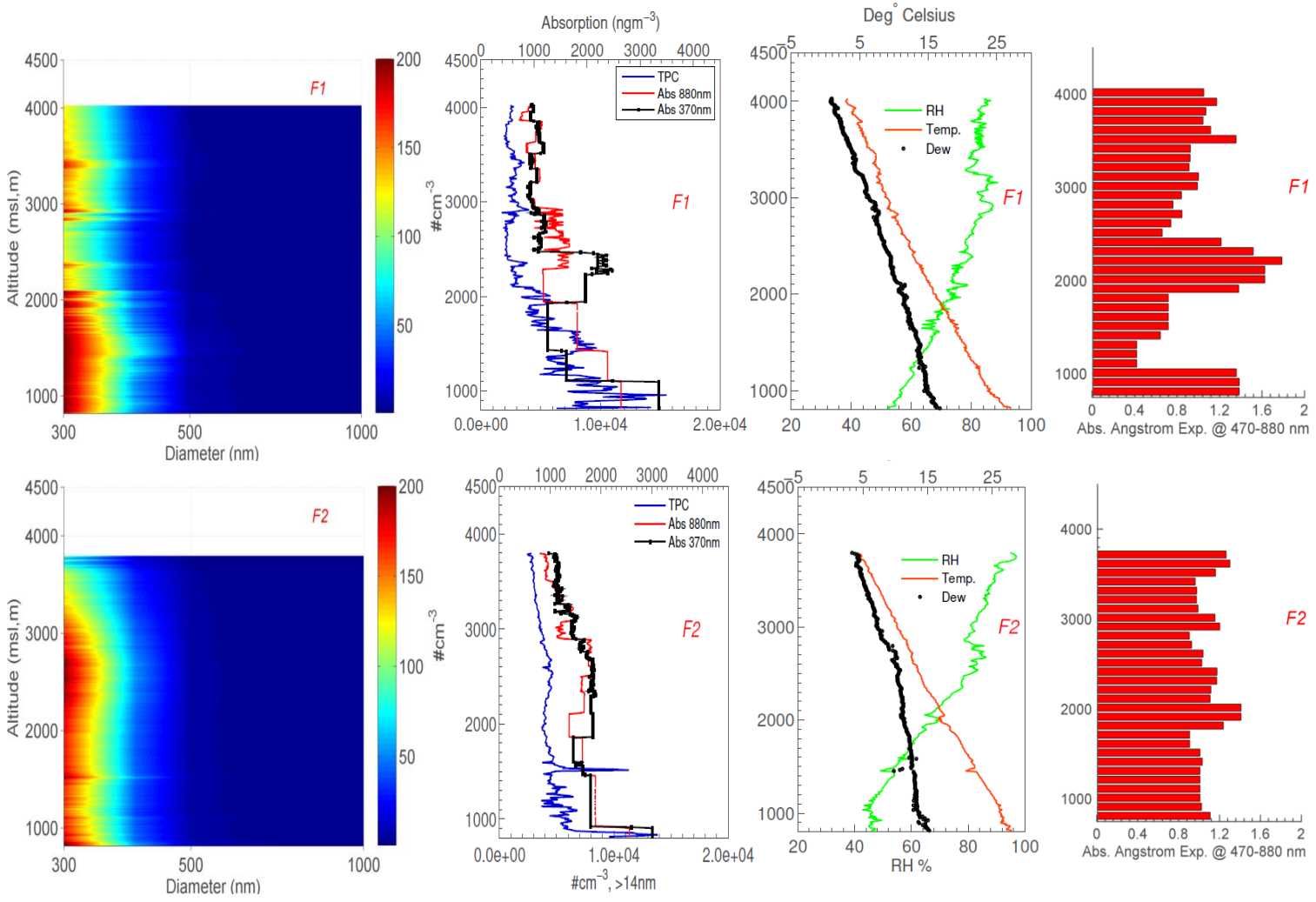
F1
Altitude (msl,m)
Diameter (nm)
Absorption (ngm$^{-3}$)
TPC
Abs 880nm
Abs 370nm
#cm$^{-3}$
Deg ° Celsius
RH
Temp.
Dew
Abs. Angstrom Exp. @ 470-880 nm
F2
#cm$^{-3}$, >14nm
RH %

688

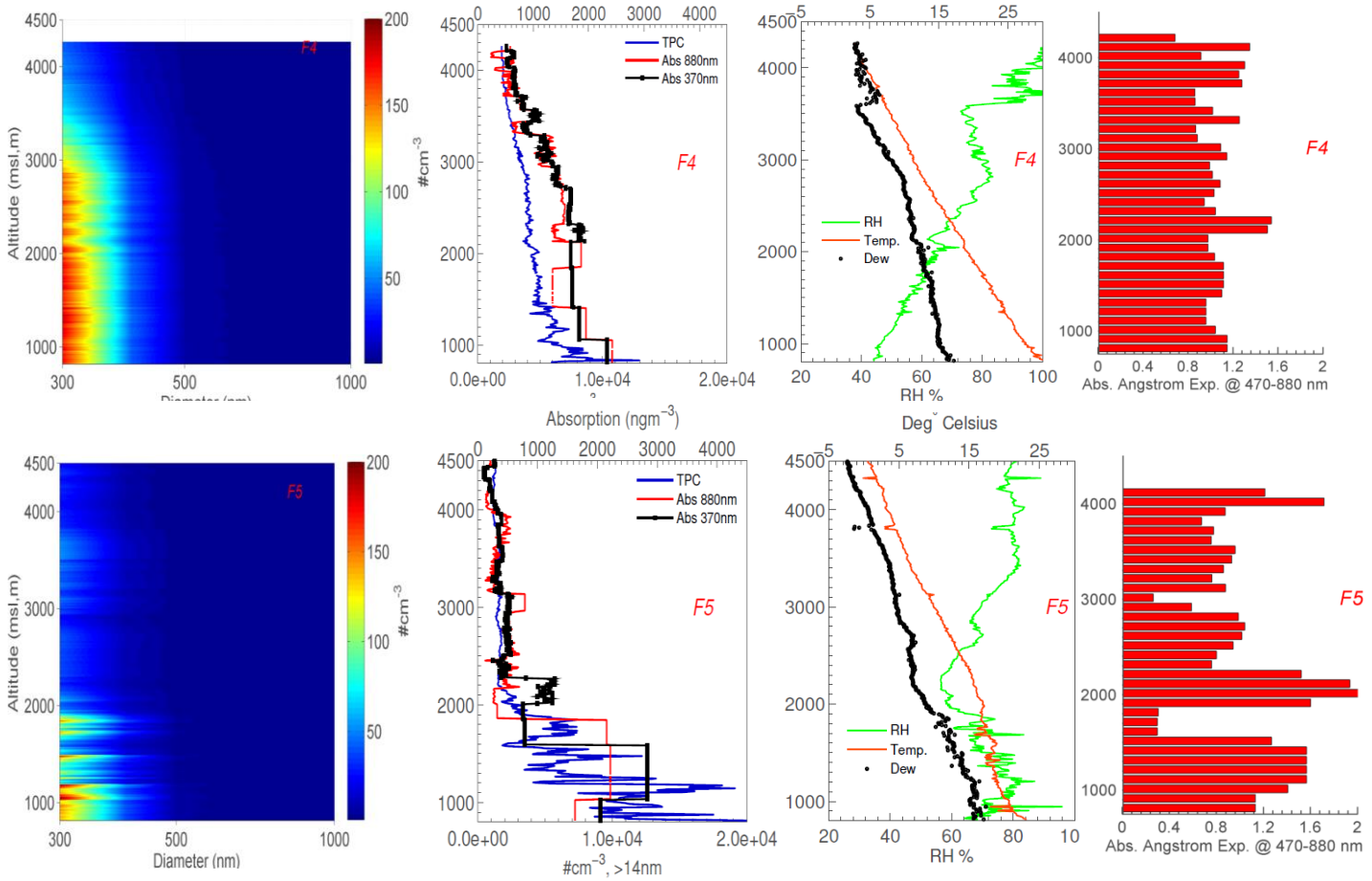


689 **Figure 4.** Vertical profiles of aerosol parameters and meteorological parameters during the 5-7 May 2016 test flights in the Pokhara Valley using
690 the IKARUS microlight aircraft. The subplot in each row is arranged by (**i**) Aerosol number size distribution measured by the Grimm OPC 1.108
691 (0.3-20 µm), limited to 1 µm in the figure, (**ii**) Total particle number concentration (also indicated as ***TPC***, Dp >14 nm) measured by the CPC 3760
692 and absorption aerosol at 370 nm and 880 nm (**iii**) temperature (°C) and dew point (black dot, in °C) and relative humidity (or RH %), (**iv**)

693 calculated absorption Ångstrom exponent averaged for every 500 meters elevation band. For the size distribution plot, the x-axis represents the
694 optical diameter of the aerosol (nm), and the color bar represents the concentration ($10^x$ in $\#cm^{-3}$). Of the five test flights, only F1-2, F4-5 is
695 shown here, F3 is in the supplementary. Number size distribution data from Flight F3 is not available due to the failure of the Grimm's pump
696 during flight initiation. In each subplot, the y-axis is the altitude above the mean sea level (in m). The origin of the y-axis is at 815 m (a.s.l.).

697

698

699

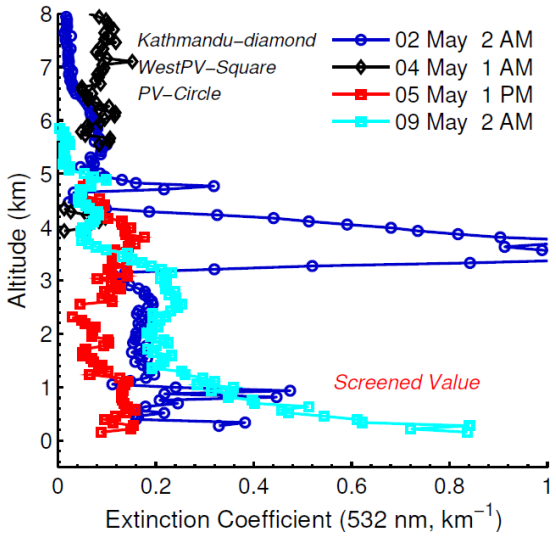


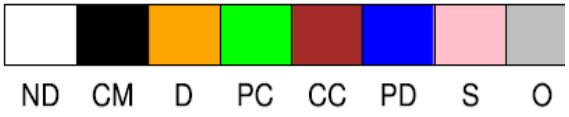


**ND**-not detected, **CM**: clean Marine, **D**:dust
**PC:** Polluted Continental, PD: Polluted Dust;
**CC**: clean continental, S: Smoke, **O**:Others

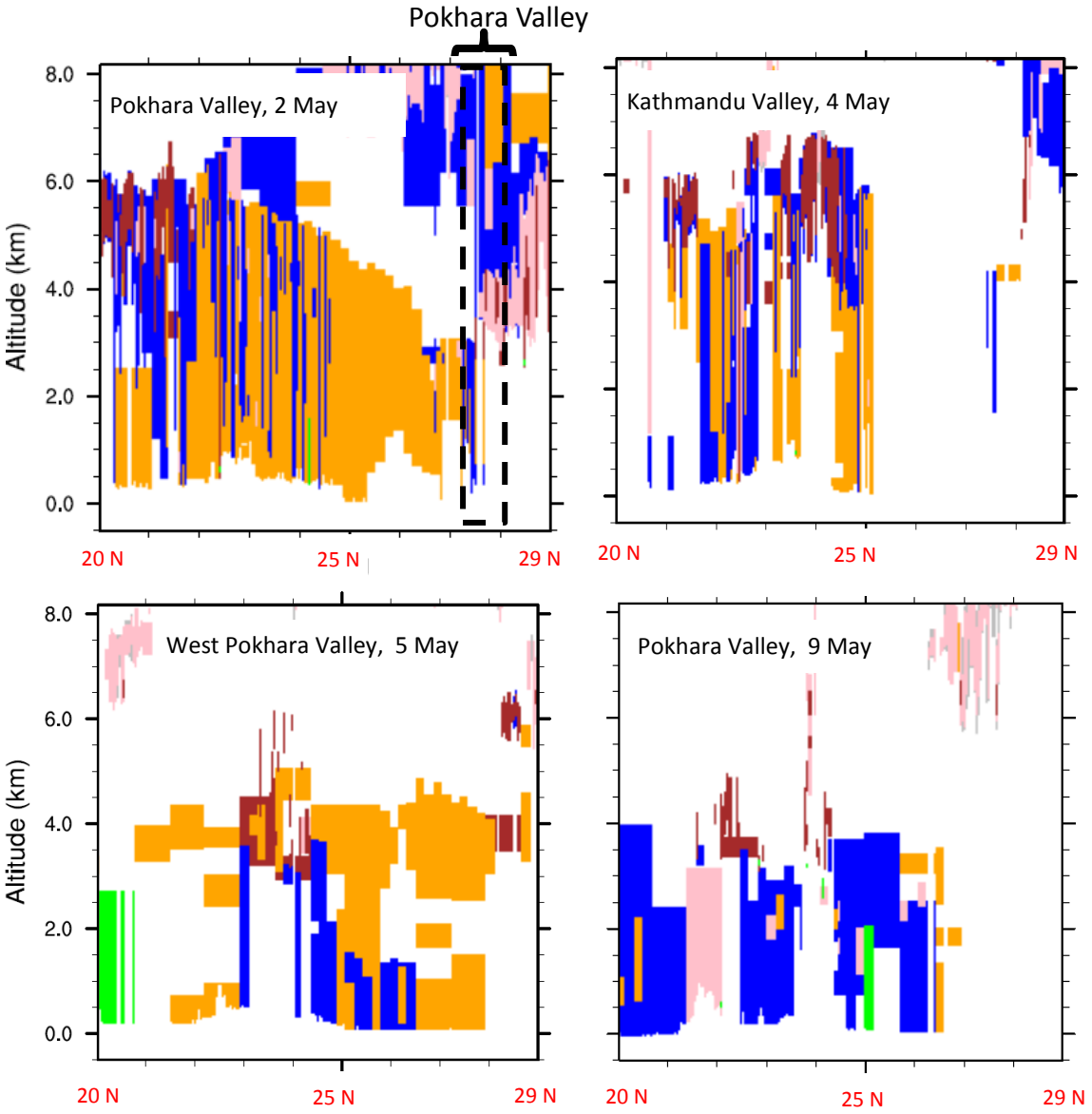


700

**Figure 5**. Aerosol extinction coefficient (at 532 nm) vertical profile (left) and aerosol type classification based on the CALIPSO level 2 retrieval (right) available during May 2016. Only the CALIPSO overpass over the Pokhara Valley or nearby locations (such as Kathmandu Valley region, and the region to west of Pokhara Valley) are included). The extinction profile is averaged for the region 27-28.5° N latitude which also includes the Pokhara Valley.

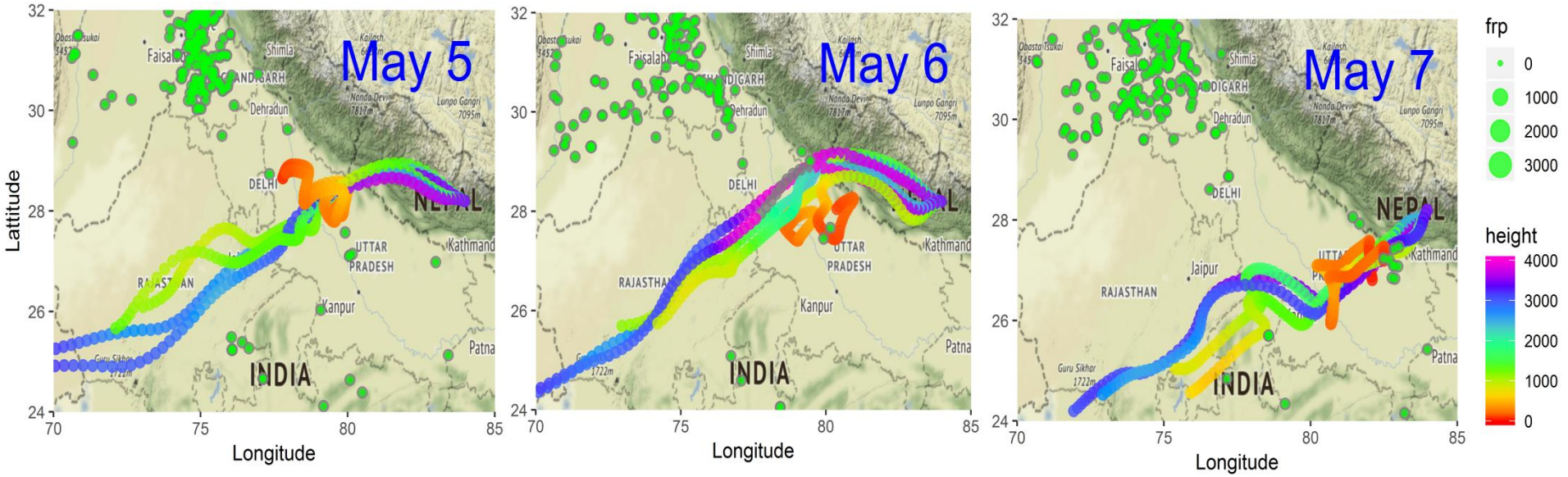


706 **Figure 6**. HYSPLIT (Hybrid Single Particle Lagrangian Integrated Trajectory) 3 day back trajectories of air masses arriving at 3 different heights
707 (800 m, 1500 m and 2500 m) from above the ground level (AGL~ 815 m a.s.l.) in the Pokhara Valley (28.19° N, 83.98° E) during 5-7 May 2016.
708 NCEP GDAS (Global Data Assimilation System) Reanalysis data with 1°x1° horizontal resolution were used as the input meteorology. The
709 trajectory data is overlayed with the active fire data (extracted from the MODIS collection 6 database, available at
710 https://firms2.modaps.eosdis.nasa.gov/active_fire/ . Each green dot with a gray edge is an active fire, and the strength of the active fire is
711 indicated by the *"frp" value,* which is the fire radiative power in megawatts.

712